Tellus (1998), 50B, 317–330
Printed in UK – all rights reserved

TELLUS
ISSN 0280–6495

Concentration, size-distribution and deposition of mineral aerosol over Chinese desert regions

By XIAO Y. ZHANG,* R. ARIMOTO[1], G. H. ZHU[2], T. CHEN and G. Y. ZHANG, *State Key Laboratory of Loess and Geology, Chinese Academy of Sciences, P.O. Box 17, Xi'an, 710054, China; [1]Carlsbad Environmental Monitoring & Research Center, New Mexico State University, 1400 University Drive, Carlsbad, NM 88220, USA; [2]Beijing Normal University, Institute of Low Energy Nuclear Physics, Beijing, 100875, China*

(Manuscript received 26 January 1998; in final form 13 May 1998)

ABSTRACT

The mass-particle size distributions (MSDs) of 9 elements in ground-based aerosol samples from dust storm (DS) and non-dust storm (N-DS) periods were determined for 12 sites in 9 major desert regions in northern China. The masses of the 9 elements (Al, Fe, K, Mg, Mn, Sc, Si, Sr and Ti) in the atmosphere were dominated by local mineral dust that averaged 270 μg m^{-3}, and the MSDs for the elements were approximately log-normal. On the basis of Al data, the <10 μm particles account for ~84% of the total dust mass over the deserts. Model-calculated ("100-step" method) dry deposition velocities (V_d) for the 9 dust-derived elements during N-DS periods ranged from 4.4 to 6.8 cm s^{-1}, with a median value of 5.6 cm s^{-1}. On the basis of a statistical relationship between $D_{99\%}$ (the dust particle diameter corresponding to the uppermost 1% of the cumulative mass distribution) and V_d, one can also predict dry velocities, especially when $D_{99\%}$ ranges from 30 to 70 μm. This provides a simple way to reconstruct V_d for dust deposits (like aeolian loess sediments in the Loess Plateau). The estimated daily dry deposition fluxes were higher during DS vs. N-DS periods, but in most cases, the monthly averaged fluxes were mainly attributable to N-DS dust. Two regions with high dust loading and fluxes are identified: the "Western High-Dust Desert" and the "Northern High-Dust Desert," with Taklimakan Desert and Badain Juran Desert as their respective centers. These are energetic regions in which desert-air is actively exchanged, and these apparently are the major source areas for Asian dust.

1. Introduction

Chinese desert regions are widely considered to be the major sources for Asian dust, for loess matter deposited on the Loess Plateau and for marine sediments in the North Pacific (Prospero, 1981; Zhang, 1984; Liu et al., 1985; Blank et al., 1985; Rea et al., 1985; Uematsu et al., 1985; Merrill et al., 1989; 1994; Zhang et al., 1996). The prevailing northwesterly winter-monsoon winds (An et al., 1991a; Zhang et al., 1998) and westerly winds (Merrill et al., 1989) from central Asia entrain the bulk of the Chinese desert dust delivered to inland China, eastern Asia, the Pacific Ocean and beyond. Scientific interest in the chemistry and fluxes of Asian dust has been stimulated because the aeolian material plays an important role in the biogeochemical cycles of trace elements in the mid-latitude Northern Hemisphere (Uematsu et al., 1985; Arimoto et al., 1989 and 1990; Zhang et al., 1993). This aeolian material also has significant impact on climate (Grassl, 1988) and the chemistry of the Pacific Ocean

* Corresponding author.
e-mail: xiaoye@loess.llqg.ac.cn.

(Orians and Bruland, 1985; Martin and Gordon, 1988; Bruland et al., 1994). Recently there has been an increasing interest in the connections among Asian dust, aeolian deposits and paleoclimate. For instance, loess sediments have been used extensively as indicators of long-term changes in the winter and summer monsoon climate of eastern Asia (An et al., 1990; 1991b; Zhang et al., 1994; Zhang et al., 1998) and variations in the large-scale atmospheric circulation in the past (Zhang et al., 1997).

Despite the biogeochemical and climatic significance of Asian dust, little information is available on the mineral dust chemistry, grain-size or fluxes in the desert-source regions. Although dust inputs are evident in Chinese loess (Liu et al., 1985; An et al., 1991b; Zhang et al., 1993; 1994; Porter and An, 1995; An and Porter, 1997), it has not been possible to estimate the dry deposition rates for mineral dust to the loess deposits or to reconstruct the dust loadings when the loess was deposited. In this paper, we present the mass particle-size distributions of 9 dust-derived elements in aerosol samples that were collected at 12 Chinese desert sites. The specific objectives of the studies were (1) to determine the concentrations of selected trace elements in the size-separated aerosol samples during dust storm (DS) and non-dust storm (N-DS) periods, (2) to characterize the mass particle-size distributions (MSDs) for mineral dust, (3) to estimate the dry deposition velocities of the elements through a "100-step" model calculation, (4) to establish a statistical relationship between a grain-size parameter and the dry velocity of dust so as to provide a basis for back calculating dust deposition, and finally (5) to characterize the dust fluxes for mineral dust over the source regions.

2. Sampling and methods

120 ground-based size-separated aerosol particle samples were collected at 12 Chinese desert sites (Fig. 1) during the spring of 1994. 9 sets of samples were collected during DS periods. Sampling intervals ranged from 4 to 8 h, and the sampling dates are listed in Table 5. Single orifice, 8-stage, Battelle-type cascade impactors (PIXE International Corporation, Tallahassee, Florida) were used for sampling. The flow rates were approximately $1\,l\,min^{-1}$, thus providing 8 particle-size fractions for the backup filter to 7th stage as follows: <0.25, 0.25 to 0.5, 0.5 to 1, 1 to 2, 2 to 4, 4 to 8, 8–16 and >16 μm in aerodynamic equivalent diameters.

Mylar® films (3.5 μm thick and coated with paraffin on stage 1 and Vaseline on stages 2 to 7) were used as the impaction surfaces, and Millipore® filters (0.4 μm porosity, Millipore, Corp., Bedford, Massachusetts) were used as the backup filters. The samples were analyzed directly using a proton induced X-ray emission (PIXE) method. The PIXE analyses were performed using the 2.5 MeV protons with a 50 nA beam current produced by 2×1.7 MV tandem accelerator at Beijing Normal University (for details see Zhang et al., 1993). Through these procedures we determined the concentrations of 9 elements: Al, Fe, K, Mg, Mn, Sc, Si, Sr and Ti. The data were corrected for backgrounds from the coated filters.

For quality control/quality assurance (QC/QA), the concentrations of the elements were determined by PIXE in 8 aliquots of a standard reference material from the National Bureau of Chemical Exploration Analysis, China (GSS, 1984). The QC/QA tests showed that both the precision ($<10\%$) and accuracy ($<20\%$) were satisfactory.

3. Results and discussion

3.1. *Elemental characterization of aerosol particles*

The concentrations of 9 elements in the surface-based aerosol samples from the desert regions are summarized in Table 1 for N-DS and DS periods. These concentrations are the sums of the data for 8 individual cascade impactor filters. One can show that the elemental composition closely resembles average crustal rock (Taylor, 1964). This is demonstrated by a calculation of enrichment factors relative to crustal rock using Al as the reference element ($EF_{crust} = (X/Al)_{air}/(X/Al)_{crust}$). The EF_{crust} values, all smaller than 5, indicate that the 9 elements in the samples were components of the mineral dust.

Not surprisingly, the concentrations of all 9 dust-derived elements were higher in the DS samples than in the N-DS samples (Table 1). The highest concentrations of the various elements were found in different DS samples, however, and this implies that the proportions of the dust ele-

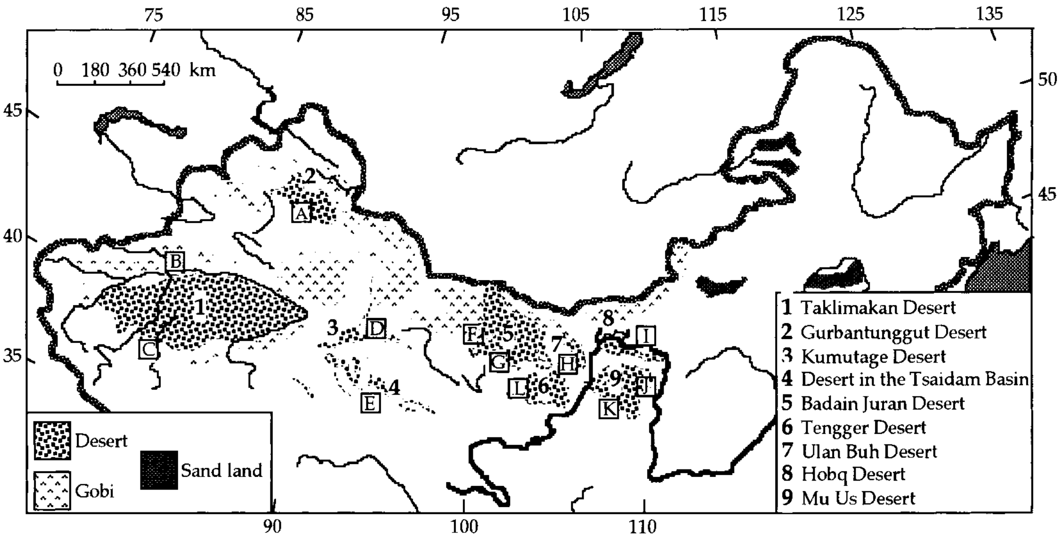

Fig. 1. Map showing the distributions of 9 major deserts in northern and northwestern China (1–9), aerosol sampling locations (A–L) in the desert regions. A. Fukang (44° 17′N, 88° 7′E), B. Aksu (41° 22′N, 80° 43′E), C. Qira (37° 6′N, 82° 34′E), D. Dunhuang (40° 16′N, 94° 10′E), E. Golmud (36° 52′N, 95° 54′E), F. Jiayuguan (40° 38′N, 98° 31′E), G. Heiquan (40° 26′N, 100° 16′E), H. Jartai (40° 34′N, 106° 34′E), I. Dalad Qi (40° 53′N, 110° 5′E), J. Yulin (38° 37′N, 109° 46′E), K. Dingbian (37° 37′N, 107° 34′E), L. Minqin (39° 17′N, 103° 10′E).

ments may vary among different Chinese desert sources. Of all the elements, Si had the highest concentration in the desert dust. At the northern margin of Taklimakan Desert (Aksu) the Si concentration reached 420 μg m^{-3} (Table 1). For most elements, the EF values increased during DS periods, indicating that local desert dust may be enriched with these elements relative to Al.

On the basis of the Al data (Al accounts for ~8% of the total mass of mineral aerosol, Taylor, 1964), the mean dust concentration over all the 12 desert sites during the spring of 1994 was 270 μg m^{-3}, with a range of 60 to 950. This is about 30% higher than that over the Chinese Loess Plateau during dry season (Zhang et al., 1993). The spring time dust concentrations over the deserts are also 3 times the mean value for the winter half-year (80 μg m^{-3}) over the Tibetan Plateau, almost 5 times higher than the locally generated dust from the Tibetan Plateau (56 μg m^{-3}), and more than 10 times higher than that observed in the mid-troposphere of remote sources (20 μg m^{-3}), respectively (Zhang et al., 1996). The dust loadings found in the present study are in fact among the highest observed over the arid and semi-arid lands in China.

3.2. *Mass particle-size distributions (MSDs) of the dust-derived elements*

We use the cascade impactor data for the 9 elements in DS and N-DS samples to compare the MSD patterns of desert dust from the source regions with the dust MSDs over the Loess Plateau (Zhang et al., 1993). Through this comparison we were able to investigate how the mass-particle-size distributions of dust particles change under different conditions. The MSD patterns are summarized in Fig. 2. In general the 9 dust-derived elements exhibited similar MSDs, and these also were similar to the MSDs for dust samples collected in the Loess Plateau (Zhang et al., 1993), suggesting that the mineral dust pulses over the loess area have close ties to the source materials from desert regions. However, more of the dust mass was associated with large particles in the source region samples during both DS and N-DS conditions. In most case particles with diameters larger than 1 μm increased disproportionately during the DS periods, indicating a lesser influence of dust storms on the masses of small dust particles.

The measurements of present-day dust have

Table 1. *Mean concentrations and enrichment factors of elements in the atmosphere of Chinese desert regions*

	Non-dust storm periods (no. samples = 111)								
	Al	Fe	Mg	Mn	K	Sc	Si	Sr	Ti
Conc. ($\mu g\ m^{-3}$)[a]	20	14	5.7	0.70	9.3	6.1×10^{-3}	80	0.09	2.2
Range	4.8–44	2.4–77	0.76–16	0.14–2.5	1.3–41	$1.8–15 \times 10^{-3}$	21–280	0.03–0.38	0.49–8.1
EFcrust (Al)[a]		0.94	1.1	2.9	1.7	1.2	1.1	1.1	1.5
Range		0.31–2.6	0.22–2.9	2.1–4.9	0.77–4.4	0.70–1.8	0.68–1.9	0.29–4.9	0.94–2.6
	Dust storm periods (no. samples = 9)								
	Al	Fe	Mg	Mn	K	Sc	Si	Sr	Ti
Conc. ($\mu g\ m^{-3}$)[a]	43	61	5.9	1.9	33	12×10^{-3}	240	0.18	6.5
Range	20–76	13–120	2.1–12	0.66–3.3	7.4–60	$5.9–19 \times 10^{-3}$	71–420	0.05–0.36	1.9–11
EFcrust (Al)[a]		1.9	0.57	3.7	2.8	1.1	1.6	0.95	2.1
Range		1.0–2.4	0.19–1.6	2.9–4.5	1.5–3.4	0.79–1.3	1.1–1.8	0.26–2.1	1.4–2.4

[a] Arithmetic mean value.

shown that particle-size distributions for mineral dust are actually composed of 3 modes, each characterized by a log-normal size distribution, with size ranges of about 20 to 200, 2 to 20, and 0.04 to 1 μm in diameter (Patterson and Gillette, 1977). Zhang et al. (1993) found that the MSDs of dust-derived elements (Al, Ca, Fe, K, Si, Ti) and non-dust elements (S and As) over the Loess Plateau were approximately log-normal. Zhang et al. (1994) also demonstrated the existence of the 3 modes in loess deposits on the Loess Plateau, with the >20 μm particle fraction (i.e., the heavy mode) mainly associated with heavy-dust transport events. Moreover, the 2–20 μm particles represented the ubiquitous dust deposited under all conditions (normal or central mode), while the <1 μm particles mainly reflected the deposition of background dust plus weathering and reworking products (background mode).

Here, the fitting of MSDs for the 9 elements is performed using the method of Zhang et al. (1993), which involves a least-squares linear regression between SND and ln *D*.

$$\mathrm{SND} = A + B \ln D, \qquad (1)$$

where SND is the standard normal deviate of the cumulative percentage of the total mass of an element of interest for each cascade impactor stage, and ln *D* is the natural logarithm of the particle diameter representing the 50% cut size for the corresponding impactor stage.

As stage 7 and the backup filter of our impactor have cut-off characteristics in the heavy mode (>20 μm) and background mode (<1 μm) particles, respectively, the fitting of monomodal log-normal distributions to our desert-sample data provides a way to assess the relative importance of giant particles and the submicrometer background dust. Generally, a standard deviation of the fitted MSD larger than 2 indicates that there are especially strong influences from heavy or background mode particles (Arimoto et al, 1985; Dulac et al., 1989; Zhang et al., 1993 and 1994).

Based on the correlation coefficients of the least-squares linear regressions, the log-normal fitting of the 9 elemental MSDs was satisfactory at the <5% probability level for 918 of 1080 size distributions. The geometric standard deviations (σ_g) of the curves generally were less than 2 (100% of the total samples for Al; 93% for Fe; 86% for Mg; 83% for Si; 79% for K, 68% for both Ti and Sr, 61% and 55% for Mn and Sc, respectively). These results indicate that there were generally minor impacts of the heavy and background mode particles on the MSDs for each element. However, in most cases both the coarser and finer dust particles were enriched with Sc, Mn, Sr, Ti, K, Si and Mg, showing some variation in composition, relative to Al and Fe, as a function of particle size.

During N-DS conditions, i.e., days on which dust was suspended in the atmosphere but dust storms were not reported as part of the routine meteorological observations, the largest differences between the samples with broad MSDs ($\sigma_g > 2$) versus the more typical ones ($\sigma_g \leqslant 2$) were due to a larger proportion of particles in the heavy mode and large values for $D_{99\%}$ (particle diameters corresponding to uppermost 1% of cumulative mass distribution). For example, for Sc the samples showing broad MSDs, had an average $D_{99\%}$ of 102 μm versus 42 μm for typical N-DS conditions (Table 2).

We believe that aerosol MSDs with large numbers of giant particles should be excluded from deposition rate calculations because those large particles have such short lifetimes that they are not likely to be transported long distances. Particles with diameters of one hundred to several hundred micrometers have been observed over the desert-source regions, but those are exceptional cases, and it is likely that most particles of that size would be deposited close to their source. Ultra giant dust particles also have been observed over the remote Pacific (Betzer et al., 1988), but the occurrence of such large dust particles could not explained based on the accepted knowledge of atmospheric transport. These authors also noted that such large particles also are extremely rare in deep-sea sediments from the North Pacific.

From the fitted MSD curves, we calculate the masses for each element in each of 3 modes (Table 3). In most cases, the mean percentages in the 3 size fractions varied little among the 9 elements during both N-DS and DS periods, suggesting that the suite of elements was carried by similar-size dust particles. Although the proportions of the elements in the heavy-dust mode (>20 μm) increased dramatically during DS periods, the 2–20 μm particles were still dominant in terms of total mass for the DS and the N-DS samples (Table 3).

Here estimates of size spectra of mineral dust

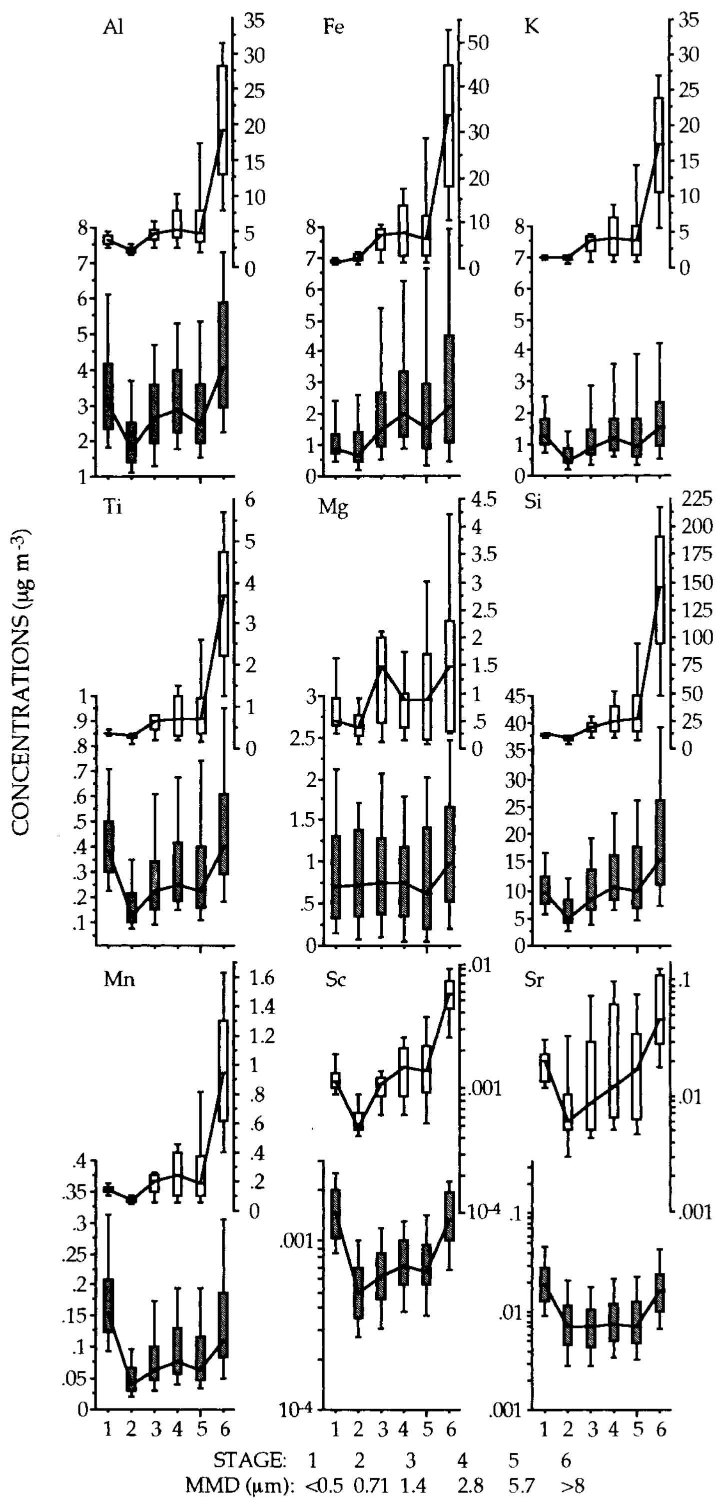
Al
Fe
K
Ti
Mg
Si
Mn
Sc
Sr
CONCENTRATIONS (μg m-3)
STAGE: 1 2 3 4 5 6
MMD (μm): <0.5 0.71 1.4 2.8 5.7 >8

Table 2. *Comparison of mass particle-size parameters for normal and broad Sc distributions for samples from the Chinese desert regions*

	Sc		
	normal MSDs (N) (σ_g[a] < 2, n[b] $= 60$)	broad MSDs (B) ($\sigma_g > 2$, $n = 51$)	B/N
<1 μm fraction (%)	38	37	1.0
range	20–60	18–62	
2–20 μm fraction (%)	55	51	1.1
range	33–75	32–64	
>20 μm fraction (%)	6.8	12	0.57
range	0.10–23	3.9–26	
$D_{(99\%)}$[c]	42	102	0.41
range	9–124	22–330	
wind speed (cm s^{-1})	192	280	
range	10–700	20–820	0.69

[a] Geometric standard deviation from log-normal fitting.
[b] Number of samples.
[c] $D_{(99\%)}$ denote particle diameter corresponding to the upper 1% of the cumulative mass distribution.

Table 3. *Arithmetic means for particle-size parameters and dry deposition velocities of dust-carrying elements over Chinese desert regions*

	Non-dust storm periods								
	Al (n[a] $= 111$)	Fe ($n = 103$)	Mg ($n = 96$)	Mn ($n = 67$)	K ($n = 87$)	Sc ($n = 60$)	Si ($n = 93$)	Sr ($n = 73$)	Ti ($n = 74$)
>20 μm fraction (%)	7.1	6.2	5.4	5.0	5.0	6.8	6.7	4.7	5.8
2–20 μm fraction (%)	55	56	57	57	57	55	55	57	56
<1 μm fraction (%)	38	38	38	38	38	38	38	38	38
V_d (cm s^{-1})	5.4	5.8	4.4	5.6	5.4	6.8	6.3	5.0	6.3
range for V_d	0.39–22	0.19–34	0.10–53	0.22–61	0.22–51	0.32–37	0.22–39	0.22–16	0.24–100
	Dust storm periods								
	Al ($n = 9$)	Fe ($n = 8$)	Mg ($n = 7$)	Mn ($n = 6$)	K ($n = 8$)	Sc ($n = 6$)	Si ($n = 7$)	Sr ($n = 8$)	Ti ($n = 7$)
>20 μm fraction (%)	19	20	7.1	22	21	22	29	11	24
2–20 μm fraction (%)	55	57	70	59	56	56	51	67	55
<1 μm fraction (%)	22	22	23	19	22	22	20	22	20
V_d (cm s^{-1})	61	33	15	45	37	57	110	18	50
range for V_d	9.4–200	8.6–140	0.42–98	10–140	9.3–79	15–96	13–350	1.6–55	11–110

[a] No. of samples.

Fig. 2. Mass particle-size distributions for trace elements in aerosol particle samples at the Chinese desert regions in spring of 1994. Open boxes denote samples collected during dust storm periods, filled boxes denote samples from the non-dust storm periods.

(based on the fitted Al MSD) in the atmosphere over the desert regions show that the mass of background dust was ~38% and 22% of the total mineral aerosol mass for N-DS and DS periods, respectively (Table 3). The heavy and normal dust modes typically contain about 7.1% and 55% of the total dust during N-DS periods, respectively; versus 19% and 55% for DS periods (Table 3). Of the total mass of the 2–20 μm particles (DS and N-DS samples, combined), about 86% was attributable to particles smaller than 10 μm, suggesting that nearly half (47%) of the total dust mass over the desert regions was carried by particles in size range of 2–10 μm.

3.3. *Dry deposition velocities for dust-derived elements*

The dry deposition flux (F) for an element can be calculated as the product of its airborne concentration (C_a) and a dry deposition velocity (V_d):

$$F = C_a V_d. \qquad (2)$$

Measurements of dry velocities in Chinese desert areas have been limited, and direct measurements are still controversial. Deposition velocities used in (2) were derived from a two-layer depositional model for the deposition of particles to smooth sticky surfaces (Slinn and Slinn 1981). The dry deposition velocity (V_d) was calculated as:

$$V_d = V_g + u_*^2//k\hat{u}(\mathrm{Sc}^{0.6} + 10^{-3/\mathrm{St}}), \qquad (3)$$

where V_g is the gravitational settling velocity; u_* is the wind friction velocity that was derived from its interrelationships with $\hat{u}$ and a drag coefficient of 0.0025, which corresponds to a steady wind at 10 m for non-water surfaces (Slinn and Slinn, 1981); $\hat{u}$ is the mean wind speed measured at the sampling locations; k is von Karman's constant (=0.4); Sc is the particle Schmidt number, and St is the particle Stokes number. Actually, at a given relative humidity (RH), there are 2 main factors, the MSD and wind speed, that determine the V_d for dust particles. The various terms used in this model were described in detail in the original papers by Slinn and Slinn (1981) and Zhang et al., (1993).

We used a 100-step approach to take the MSDs of a dust element into the calculation of dry depositional flux. This depends on the fitting of a continuous distribution to cascade impactor data (Arimoto et al., 1985; Dulac et al., 1989; Zhang et al., 1993). Using model-derived dry deposition velocities and measured elemental concentrations, the dry deposition fluxes were calculated as:

$$F_{100} = \sum_{i=1}^{100} (C_a/100) V_d[D_{(i-0.5)\%}], \qquad (4)$$

where $V_d[D_{(i-0.5)\%}]$ is the dry deposition velocity for a particle in the center of each of the 100 particle-size intervals i. A consequence of this discrete representation of a lognormal distribution is that the mass of each element is divided among a finite number of size classes, and these sizes range over the diameters corresponding to 0.5 and 99.5 of the cumulative mass. The results of Arimoto et al. (1985), Dulac et al. (1989) demonstrate that the 100-step method can produce realistic dry deposition rates.

The mean dry deposition velocities (v) integrated over the entire MSDs for each element are presented in Table 3. These were derived from the flux calculations (F_{100}) using the 100-step method, based on the relationship:

$$v = F_{100}/C_a. \qquad (5)$$

For the Chinese desert-dust samples, the v values for the 9 elements were quite similar during N-DS conditions, 4.4 cm s^{-1} for Mg to 6.8 cm s^{-1} for Sc in Table 3, and this reflects the fact that they all were carried by similar-size dust particles. The mean v for the dust-elements in the desert samples (5.6 cm s^{-1}) is about 60% higher than the dry deposition velocity for dust-derived elements at the Loess Plateau (3.5 cm s^{-1}, range of 3.3 to 3.7 cm s^{-1}, Zhang et al., 1993), and it twice that of Beijing samples from the high dust season (2.1 cm s^{-1}, Zhang et al., 1993). During DS periods, the mean V_ds of the elements increased in conjunction with a higher proportion of heavy-mode particles. This increase in V_d was not observed for Fe, however, perhaps due to the relatively small number giant particles apparently associated with Fe and the small amount of DS data used for averaging.

3.4. *Relationship between $D_{99\%}$ and dry deposition velocity for mineral dust particles*

When calculating deposition rates, it is essential to consider the entire MSDs, and this is why we used the "100-step" method. However, because coarse particles contribute disproportionately to dry deposition (Slinn, 1981; Arimoto et al., 1985; Dulac et al., 1989; Zhang et al., 1993), one might expect that a suitable coarse particle index could be related to the flux rates. If this relationship were validated, one could then apply the technique to back calculate dry deposition rates from the analysis of the dust deposits, such as loess sediments.

The >20 μm fractions and $D_{99\%}$ of mineral dust (based on Al data) exhibit similar variations (correlation coefficient, $r=0.93$) that had little or relationship to wind speed ($r=0.17$ and 0.13 for the 2 parameters versus wind speed, respectively). This was true for the combined DS and N-DS data, and for the DS and N-DS data separately. Similarly, there was no relationship between the 2 particle size indexes and dust loading. Therefore, the proportion of heavy-mode particles and the larger $D_{99\%}$s for mineral dust are at most weakly related to wind speed, and as a result there is no close relation to dust loading.

As was true for the $D_{99\%}$ and >20 μm fractions of dust, the variations of "100-step" model-derived dry velocities (V_d) were weakly related to wind speed if at all ($r=0.18$ for the 2 parameters). However, the V_d variations of dust were strongly related to the >20 μm dust-size fraction and especially $D_{99\%}$ in most cases. This is demonstrated by the fact that $D_{99\%}$ and the percentage of heavy mode particles were highly correlated with V_d. Because of the high correlation for $D_{99\%}$ ($r=0.86$), only the statistical relationship between $D_{99\%}$ versus V_d for dust particles (based on Al data) is presented in Fig. 3a. The $D_{99\%}$ values used in the regression ($n=101$) are those ranging from 18 to 66 μm and corresponding to more than 86% of the total counts in frequency distribution analysis; these are considered to be representative of the dust loadings under most general conditions (Fig. 3b). In comparison, the $D_{99\%}$s for loess sediments from the last glacial and interglacial cycles ranged from 33 to 66 μm (data from Zhang et al. (1994); therefore, the aerosol data selected for the fitting overlap the size of dust deposited onto the loess area.

Using the least-squares regression equation for the relationship

$$V_d = 0.235 D_{99\%} - 3.65\,, \qquad (6)$$

we then predicted the V_d for aerosol samples from the Loess Plateau and at a desert site (Shapuotou) from 1990 to 1991 and for aerosol samples collected at the desert regions during 1994. The $D_{99\%}$ data, segregated into 8 subgroups, are derived from fitted Al MSDs (Zhang et al., 1993 and this work, respectively, Table 4). For $D_{99\%}$ in the range of 30 to 70 μm (groups 3 to 6), the dry deposition rates, predicted from Equation 6, are normally with 20% of the deposition we estimated using the "100-step" method (Zhang et al., 1993 and this work, respectively; Table 4).

We consider the agreement in deposition rates remarkable, especially considering the uncertainties associated with the cascade impactor data and the meteorological measurements. For $D_{99\%}$ in the range of 20 to 30 μm (group 2), and 70 to 80 μm (group 7), differences for the 2 predicted deposition velocities are larger, of the order of 30 to 40% (Table 4). For the sample MSDs with $D_{99\%}$ less than 20 μm or larger than 80 μm (groups 1 and 8), respectively, the differences are larger yet, but still within a factor of ~ 2 (maximum value of 3.4). Therefore, the predictions of dry deposition rates simply by using $D_{99\%}$ data for mineral dust appear comparable to more sophisticated methods, especially when $D_{99\%}$ is 30 to 70 μm. The wind speeds and RHs used in the model are generally representative of arid and semi-arid regions (Zhang et al., 1993), but we note that uncertainties still exist in the $D_{99\%}$-based prediction, especially when $D_{99\%} < 20$ μm or > 80 μm. Of course, further studies are needed to improve upon the preliminary analyses presented here.

In most cases, the mineral dust samples with $D_{99\%}$ larger than 40 μm are associated with a mean wind speed greater than 3.0 m s^{-1} (Table 4). It is tantalizing to imagine that one could predict wind speeds from an aerosol grain-size index. Even though these relationships between modern-day dust and wind speeds have not been rigorously evaluated, some attempts have been made to reconstruct paleowinds or the vigor of atmospheric circulation from grain-size data for sedimentary materials (Rea et al, 1985; Rea, 1994).

3.5. *Depositional flux of mineral dust*

The depositional flux of the desert dust was parameterized as the product of dry deposition velocity and the concentration of Al based on the assumption that Al is about 8% of mineral dust by weight (Taylor, 1964). Wet deposition was not

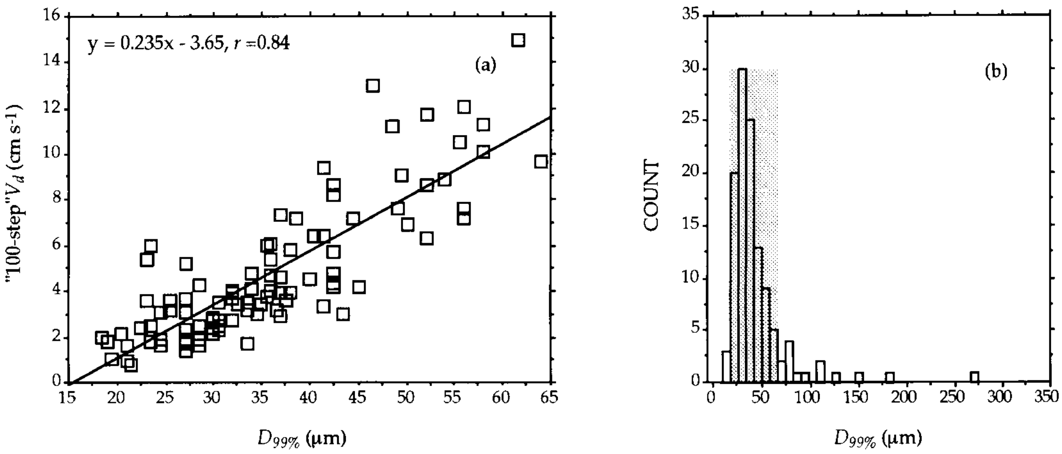

Fig. 3. (a) Statistical relationship between $D_{99\%}$ (the dust particle diameter corresponding to the uppermost 1% of the cumulative mass distribution) and "100-step" model-derived dry deposition velocities (V_d) for mineral dust; (b) Frequency distribution of $D_{99\%}$ data for mineral dust. The sizes for 101 $D_{99\%}$ data, 86% of the total counts (shadow area), range from 18 to 66 µm. All the data in (a) and (b) were derived from Al MSD data.

included in these estimates of total deposition because of the amount of precipitation in these hyperarid desert regions is extremely low (<200 mm per year with minima of 10 to 30 mm in this region, Liu et al. (1985)). The monthly deposition rates in spring for all the representative desert sites were calculated as product of the mean of daily fluxes and the corresponding numbers of days in N-DS and DS conditions (Table 5). The mean concentrations for bulk desert dust also are summarized in Table 5.

The dust fluxes over the deserts for dust-storm days were high as expected; however, in most cases the monthly DS fluxes were smaller than those due to N-DS days (Table 5). Under N-DS conditions the dust deposition rates at the various desert sites were similar to within a factor of ~4 (Table 5); in comparison, during DS conditions the range for fluxes among different sites was larger, a factor of 18, illustrating the heterogeneity of the dust loadings and fluxes.

The highest monthly flux (110 g m^{-2} mo^{-1}) for the combined DS and N-DS conditions was calculated for the southern margin of the Taklimakan Desert (Table 5). The 2 lowest fluxes and concentrations were found at Fukang and Golmud, located in Gurbantunggut Desert and the Desert in the Tsaidam Basin, respectively.

Two regions (I and II) with high dust fluxes can be seen in Fig. 4. One we refer to as the "Western High-Dust Desert" with the Taklimakan Desert at its center. The second high-dust region is composed of the deserts lying in northern Inner Mongolia and the deserts close to the northwestern margin of the Loess Plateau, with Badain Juran Desert as it center; collectively these are referred to as the "Northern High-Dust Desert." In a series of studies in the Chinese Loess Plateau, Zhang (1993) found the yearly mean dust concentration to be 170 µg m^{-3}. These levels are similar to those measured over the 2 non-active deserts, the Gurbantunggut Desert (160 µg m^{-3}) and Desert in the Tsaidam Basin (190 µg m^{-3}); this is evidence that these 2 deserts probably are not energetic regions relative to other deserts in which desert-air is more actively exchanged.

The mean dust loading and fluxes over the Western High-Dust Desert, i.e., the averages of the values for Aksu, Qira and Dunhuang, were 370 µg m^{-3} and 72 g m^{-2} mo^{-1}, respectively. The corresponding data for the Northern High-Dust Desert, averaging the data for Jiayuguan, Heiquan, Jartai, Dalad Qi, Yulin, Dingbian and Minqin, were 270 µg m^{-3} and 50 g m^{-2} mo^{-1}. The concentrations and the fluxes of dust over the Chinese deserts are much higher than those over the Loess Plateau (Zhang et al., 1993), demonstrating once again that it is the desert regions in China not the Loess Plateau that are the main sources for Asian dust.

Table 4. *Comparison of dry deposition velocities (V_d) for Al from $D_{99\%}$-based prediction versus "100-step" model estimate for the aerosol samples from the Loess Plateau (Zhang et al., 1993) and Chinese desert regions*

				Dry deposition velocity		
$D_{99\%}$ subset	no. samples	$D_{99\%}$ (μm)	wind speed (m s^{-1})	"100-step" model derived (D) (cm s^{-1})	"$D_{99\%}$" predicted (P)[a] (cm s^{-1})	D/P
subset 1: <20 μm	3	18 (18–19)[b]	2.7 (1.6–3.5)	1.6 (0.9–2.0)	0.69 (0.58–0.80)	2.2 (1.6–2.9)
subset 2: 20–30 μm	28	25 (20–29)	2.6 (1.0–5.0)	3.0 (1.0–6.0)	2.0 (0.90–3.0)	1.3 (0.63–3.0)
subset 3: 30–40 μm	28	34 (30–39)	2.4 (1.0–4.6)	4.3 (2.4–7.4)	4.4 (3.4–5.4)	1.0 (0.69–1.5)
subset 4: 40–50 μm	15	44 (40–50)	3.4 (1.5–8.2)	7.4 (4.4–13)	6.7 (5.8–8.0)	1.1 (0.70–1.8)
subset 5: 50–60 μm	9	54 (50–58)	2.7 (1.2–5.2)	9.6 (6.3–12)	9.1 (8.1–10)	1.1 (0.73–1.4)
subset 6: 60–70 μm	6	65 (61–69)	3.4 (1.9–5.4)	14 (10–21)	12 (11–13)	1.2 (0.85–1.7)
subset 7: 70–80 μm	4	76 (74–77)	3.1 (1.7–3.7)	20 (18–22)	14 (14–14)	1.4 (1.2–1.5)
subset 8: >80 μm	7	139 (85–271)	3.1 (1.3–5.6)	68 (19–203)	29 (16–60)	2.0 (1.2–3.4)

[a] See text for description of $D_{99\%}$-based prediction.
[b] Arithmetic mean (range).

Table 5. *Representative fluxes and mass concentrations of mineral dust in the air of Chinese desert regions*

Chinese Deserts	Representative Sites	n[b]	Total Fluxes[a] (mg m^{-2} mo^{-1})	Dust Conc. (μg m^{-3})	Sampling Date
Taklimakan Desert	Qira	9	33 (5.4–120)	370	5/21–23/94
	Qira-Dust storm	4	77 (31–170)	620	5/24–25/94
	Aksu	9	59 (11–260)	290	5/29–30/94; 6/1/94
	Aksu-Dust storm	3	12 (7.7–17)	600	5/31/94
Gurbantunggut Desert	Fukang	15	14 (4.3–31)	160	5/16–21/94
Desert in the Tsaidam Basin	Golmud	15	26 (7.9–54)	190	6/8–12/94
Kumutage Desert	Dunhuang	7	36 (4.5–130)	250	5/8–13/94
Badain Juran Desert	Jiayuguan	6	43 (14–87)	220	4/29–30/94; 5/2–5/94
	Jiayuguan-Dust storm	1	4.3	240	5/1/94
	Heiquan	7	27 (8.9–84)	220	5/7–10/94
Ulan Buh Desert	Jartai	6	71 (1.5–230)	260	5/16–18/94
	Jartai-Dust storm	1	37	370	5/15/94
Hobq Desert	Dalad Qi	8	47 (8.3–65)	210	5/21–23/94
Mu Us Desert	Yulin	10	44 (11–200)	310	5/26–29/94
	Dingbian	10	42 (4.1–98)	380	6/1–4/94
Tengger Desert	Minqin	9	33 (1.7–140)	200	4/23–26/94

[a] Mean value with the range in parentheses.
[b] Number of samples.

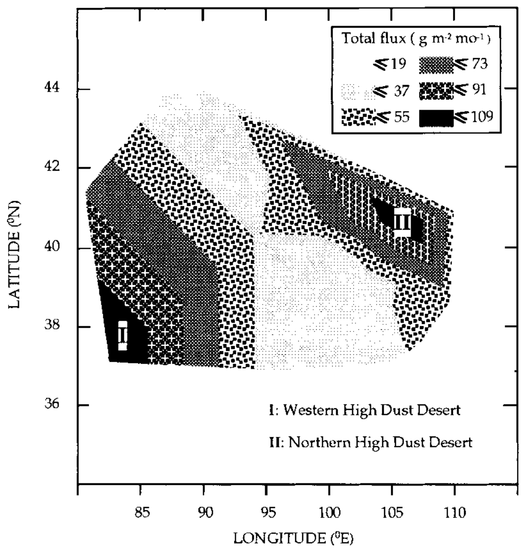

Fig. 4. Spatial distribution of monthly mean fluxes for mineral dust deposited in Chinese desert regions during Spring of 1994.

4. Conclusions

Measurements of aerosol samples in Chinese desert regions have provided the a relatively large data set for MSDs of dust-derived elements in the atmosphere over the source regions for Asian dust. The data have enabled us to characterize the loadings, mass particle-size distributions, and depositional fluxes of the source dust.

On the basis of Al data, the mean dust loadings over all the 12 desert sites (270 μg m^{-3}) were among the highest observed over arid or semi-arid areas of China. The proportions of dust in the background (<1 μm) and heavy modes (>20 μm) during N-DS conditions were ~38% and 7.1% of the total mass, respectively, and during DS conditions the corresponding figures were ~22% and 19%. Generally most of the dust mass was in the central mode (2 to 20 μm), and more than 80% of the total dust mass was carried by particles whose diameters were smaller than 10 μm.

Dry deposition velocities (V_ds) of dust were calculated by using a two-layer dry deposition model with a "100-step" method. Comparisons between the V_d and a grain-size parameter for dust have once again highlighted the major role played by coarse particles in the dry deposition process. Deposition velocities predicted from $D_{99\%}$ value agree with the those derived from the "100-step" model, especially when $D_{99\%}$ falls within a range of 30 to 70 μm. This relationship provides a simple way to reconstruct V_d for dust deposition from loess or other sedimentary materials. Of course, more studies of present-day dust need to be made to test the relationship between $D_{99\%}$ and V_d.

Depositional fluxes, which integrated the contributions of "100-step" model-derived V_d and dust loading, indicate that there are 2 active dust regions with higher dust fluxes, named "Western High-Dust Desert" and "Northern High-Dust Desert" with the Taklimakan Desert and Badain Juran Desert as their centers, respectively. These regions actively exchange desert-air with the free troposphere, and presumably they are the major source areas for Asian dust.

5. Acknowledgements

This research was supported by grants from "Ninth Five-Year Climbing Plan" of the State Science and Technology Commission of China, the Key Projects of Chinese Academy of Sciences, NSF of China, NSF ATM97–28983. We wish to thank two reviewers for their critical comments which improved the original manuscript.

REFERENCES

An, Z. S. and Porter, S. C. 1997. Millennial-scale climatic oscillations during the last interglaciation in central China. *Geology* **25**, 603–606.

An, Z. S., Kukla, G., Porter, S. C. and Xiao, Y. L. 1991a. Magnetic susceptibility evidence of monsoon variation on the Loess Plateau of central China during the last 130,000 years. *Quaternary Research* **36**, 29–36.

An, Z. S., Kukla, G., Porter, S. C. and Xiao, J. L. 1991b. Late Quaternary dust flow on the Chinese Loess Plateau. *Catena* **18**, 125–132.

An, Z. S., Liu, T. S., Lu, Y. C., Porter, S. C., Kukla, G., Wu, X. H. and Hua, Y. M. 1990. The long-term paleomonsoon variation recorded by the loess-paleosol sequence in central China. *Quaternary International* **718**, 91–95.

Arimoto, R., Duce, R. A., Ray, B. J. and Unni, C. K. 1985. Atmospheric trace elements at Enewetak Atoll, 2, Transport to the ocean by wet and dry deposition. *J. Geophys. Res.* **90**, 2391–2408.

Arimoto, R., Duce, R. A. and Ray, B. J. 1989. Concentrations, sources and air-sea exchange of trace elements in the atmosphere over the Pacific Ocean. In: *Chemical oceanography*, vol. 10 (ed. J. P. Riley, R. Chester and R. A. Duce). Academic, San Diego, Calif., 107–149.

Arimoto, R., Gao, Y., Duce, R. A., Lee, D. S. and Chen, L. Q. 1990. *International Conference on Global and regional environmental atmospheric chemistry, Preceedings*. (ed. L. Newman, W. Wang and C. S. Kiang), US Dept. of Energy, 24–40.

Betzer, P. R., Carder, K. L, Duce, R. A., Merrill, J. T., Tindale, N. W., Uematsu, M., Costello, D. K., Young, R. W., Feely, R. A., Breland, J. A., Bernstein, R. E., and M Greco, A. 1988. Long-range transport of giant mineral aerosol particles, *Nature* **336**, 568–571.

Blank, M., Leinen, M. and Prospero, J. M. 1985. Major Asian inputs indicated by the mineralogy of aerosols and sediments in the western North Pacific. *Nature* **314**, 84–86.

Bruland, K. Orians, K. J. J. P. Cowen, 1994. Reactive trace metals in the stratified central North Pacific. *Geochim. Cosmochim. Acta* **58**, 3171–3182.

Dulac, F., Buat-Ménard, P., Ezat, U., Melki, S. and Bergametti, G. 1989. Atmospheric input of trace metals to the western Mediterranean: uncertainties in modelling dry deposition from cascade impactor data. *Tellus* **41B**, 362–378.

Grassl, H. 1988. What are the radiative and climatic consequences of the changing concentration of atmospheric aerosol particles. In: *The changing atmosphere* (ed. F. S. Rowland and I. S. A. Isaksen). J. Wiley & Sons, Chichester, England, 187–199.

GSS. 1984. *Preparation of geochemical standard reference samples (GSR1–6, GSS1–8, GSD9–12)*. National Bureau of Chemical Exploration Analysis, Beijing.

Liu, T. S. et al. (unnamed) 1985. *Loess and the environment*. Ocean Press, Beijing, 157–161.

Martin, J. H. and Gordon, R. M. 1988. Northeast Pacific iron distributions in relation to phytoplankton productivity. *Deep Sea Res.* **35**, 177–196.

Merrill, J. T., Uematsu, M., Bleck, R. 1989. Meteorological analysis of long range transport of mineral aerosol over the North Pacific. *J. Geophys. Res.* **94**, 8584–8598.

Merrill, J. T., Arnold, E., Leinen, M., Weaver, C. 1994. Mineralogy of aeolian dust reaching the North Pacific Ocean: 2. Relationship of mineral assemblages to atmospheric transport patterns. *J. Geophys. Res.* **99**, 21,025–21,032.

Orians, K. J. and Bruland, K. W. 1985. Dissolved aluminum in the central North Pacific. *Nature* **316**, 427–429.

Patterson, C. C. and Gillette, D. A. 1977. Commonalities in measured size distributions for aerosols having a soil-derived component. *J. Geophys. Res.* **82**, 2074–2082.

Porter, S. C., and An, Z. S. 1995. Correlation between climate events in the North Atlantic and China during the last glaciation. *Nature* **375**, 305–308.

Prospero, J. M. 1981. Eolian transport to the world ocean. In: *The sea*, ed. C. Emiliani, vol. 7, pp. 801–874. New York: Wiley.

Rea, D. K. 1994. The paleoclimatic record provided by eolian deposition in the deep sea — the geologic history of wind. *Rev. Geophysics 32*, 159–195.

Rea, D. K., Leinen, M. and Janecek, T. R. 1985. Geological approach to the long-term history of atmospheric circulation. *Science* **227**, 721–725.

Slinn, S. A. and Slinn, W. G. N. 1981. Modelling of atmospheric particulate deposition to natural water. In: *Atmospheric pollutants in natural waters*, (ed. S. J. Eisenreich). Ann Arbor Science, Michigan, 23–53.

Taylor, S. R. 1964. Abundance of chemical elements in the continental crust: a new table. *Geochim. Cosmochim. Acta* **28**, 1273–1285.

Uematsu, M., Duce, R. A. Prospero, J. M., Chen, L., Merrill, J. T. and McDonald, R. L. 1985. Transport of mineral aerosol from Asia over the North Pacific Ocean. *J. Geophys Res.* **88**, 5343–5352.

Zhang, D. E. 1984. Synoptic-climatic studies of dust fall in China since the historic times. *Scientia Sinica* **27**, 825–836.

Zhang, X. Y., Arimoto, R., An, Z. S., Chen, T., Zhang, G., Zhu, G. and Wang, X. 1993. Atmospheric trace elements over source regions for Chinese dust: concentrations, sources and atmospheric deposition on the Loess Plateau. *Atmospheric Environment* **27A**, 2051–2067.

Zhang, X. Y., Arimoto, R., An, Z. S., Chen, T. and Zhang, G., Ray, B. J. 1994. Late Quaternary records of the atmospheric input of eolian dust to the Center of the Chinese Loess Plateau. *Quaternary Research* **41**, 35–43.

Zhang, X. Y., Arimoto, R. and An, Z. S. 1997. Dust emission from Chinese desert sources linked to variations in atmospheric circulation. *J. Geophys. Res.* **102**, 28,041–28,047.

Zhang, X. Y., Shen, Z., Zhang, G., Chen, T. and Liu, H. 1996. Remote mineral aerosol in westerlies and their contributions to Chinese loess. *Science in China* (Ser. D) **39**, 67–76.

Zhang, X. Y., Arimoto, R. and An, Z. S. 1998. Glacial and intergalcial patterns for Asian dust transport. *Quant. Sci. Res.* **17**, in press.